JACS
JOURNAL OF THE AMERICAN CHEMICAL SOCIETY
pubs.acs.org/JACS
Article

Nitrite Formation at a Diiron Dinitrosyl Complex

Anna L. Poptic, Jeffrey K. Klinger, Samantha L. Carter, Curtis E. Moore, and Shiyu Zhang*

Cite This: J. Am. Chem. Soc. 2023, 145, 22993−22999
Read Online
ACCESS | Metrics & More | Article Recommendations | Supporting Information

ABSTRACT: Pathogenic bacteria employ iron-containing enzymes to detoxify nitric oxide ($NO^{\bullet}$) produced by mammals as part of their immune response. Two classes of diiron proteins, flavodiiron nitric oxide reductases (FNORs) and the hemerythrin-like proteins from mycobacteria (HLPs), are upregulated in bacteria in response to an increased local $NO^{\bullet}$ concentration. While FNORs reduce $NO^{\bullet}$ to nitrous oxide (N_2O), the HLPs have been found to either reduce nitrite to $NO^{\bullet}$ (YtfE), or oxidize $NO^{\bullet}$ to nitrite (*Mka*-HLP). Various structural and functional models of the diiron site in FNORs have been developed over the years. However, the $NO^{\bullet}$ oxidation reactivity of *Mka*-HLP has yet to be replicated with a synthetic complex. Compared to the FNORs, the coordination environment of the diiron site in *Mka*-HLP contains one less carboxylate ligand and, therefore, is expected to be more electron-poor. Herein, we synthesized a new diiron complex that models the electron-poor coordination environment of the *Mka*-HLP diiron site. The diferrous precursor $\mathbf{Fe^{II}Fe^{II}}$ reacts with $NO^{\bullet}$ to form a diiron dinitrosyl species ($\{\mathbf{FeNO}\}^7_2$), which is in equilibrium with a mononitrosyl diiron species ($\mathbf{Fe^{II}}\{\mathbf{FeNO}\}^7$) in solution. Both complexes can be isolated and fully characterized. However, only oxidation of $\{\mathbf{FeNO}\}^7_2$ produced nitrite in high yield (71%). Our study provides the first model that reproduces the $NO^{\bullet}$ oxidase reactivity of *Mka*-HLP and suggests intermediacy of an $\{\mathbf{FeNO}\}^6/\{\mathbf{FeNO}\}^7$ species.

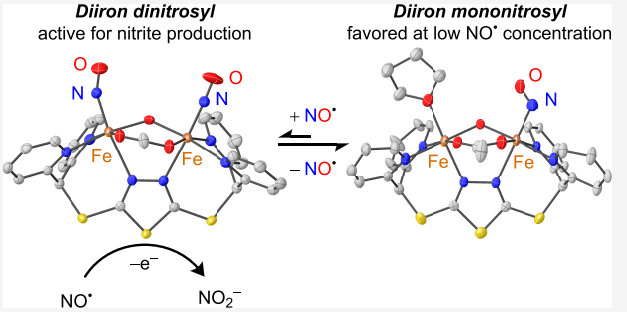

INTRODUCTION

The production of nitric oxide ($NO^{\bullet}$) by the immune system is one of the first levels of defense against an invading pathogen in the human body.[1] The reaction of $NO^{\bullet}$ with transition metal ions or superoxide produces various reactive nitrogen species (RNS) that kills the invading pathogen.[2,3] To counter the toxicity of $NO^{\bullet}$, pathogenic bacteria employ iron-containing enzymes to detoxify $NO^{\bullet}$.[4−13] The enzymes associated with this process have also been labeled as potential therapeutic targets for RNS-resistant pathogens.

One example of an $NO^{\bullet}$-detoxifying iron enzyme is the flavodiiron nitric oxide reductases (FNORs),[14] which catalyze the reduction of $NO^{\bullet}$ to nontoxic nitrous oxide (N_2O).[15,16] FNORs employ a nonheme diferrous active site (Figure 1A) to bind two $NO^{\bullet}$ molecules sequentially to form a diiron mononitrosyl ($Fe^{II}\{FeNO\}^7$)[17] and a diiron dinitrosyl $\{FeNO\}^7_2$ intermediate. Mechanistic investigations have shown that the diiron dinitrosyl is the active intermediate from which N_2O is released.[18,19] The exact order of N_2O release and electron/proton transfer is still under investigation, but ultimately, one equivalent of N_2O and one equivalent of water are produced, and the diferrous active site is regenerated.[20]

Small-molecule models of the FNOR diiron sites have proven essential in understanding the mechanism of N_2O release.[14,20,21] Lehnert et al.,[22−25] Majumdar et al.,[26−28] Lippard et al.,[29,30] Liaw et al.,[31,32] and Meyer et al.[33] have developed structural and functional models of the diiron site in FNORs (Figure 1C). Factors leading to fast and efficient N_2O release from the diiron center, including an electron-rich ligand environment and close N···N distances, have been identified.

More recently, a new class of nonheme diiron enzymes, the hemerythrin-like proteins (HLPs), were identified as participants in the nitrosative stress response. HLPs are widely distributed across taxonomic groups and have been characterized in several different organisms.[34] Similar to the diiron protein hemerythrin, HLPs were believed to participate in oxygen binding/sensing, but the structural characterization and follow-up studies of an HLP from the bacteria *E. coli*, YtfE, revealed that YtfE catalyzes the reduction of nitrite (NO_2^-) to $NO^{\bullet}$.[35,36] The $NO^{\bullet}$ produced is further reduced to generate N_2O by the hybrid cluster protein (Hcp). Shortly after the discovery of the function of YtfE, a second subclass of HLP was characterized from different species of mycobacteria (*Mka*-HLP), first from *M. tuberculosis*[37] and then *M. kansasii* (Figure 1B).[38] In contrast to FNORs and YtfE, *Mka*-HLP functions as a $NO^{\bullet}$ oxidase and converts $NO^{\bullet}$ to nitrite.[39,40] Before these

Received: May 17, 2023
Published: October 10, 2023

https://doi.org/10.1021/jacs.3c05155
J. Am. Chem. Soc. 2023, 145, 22993−22999

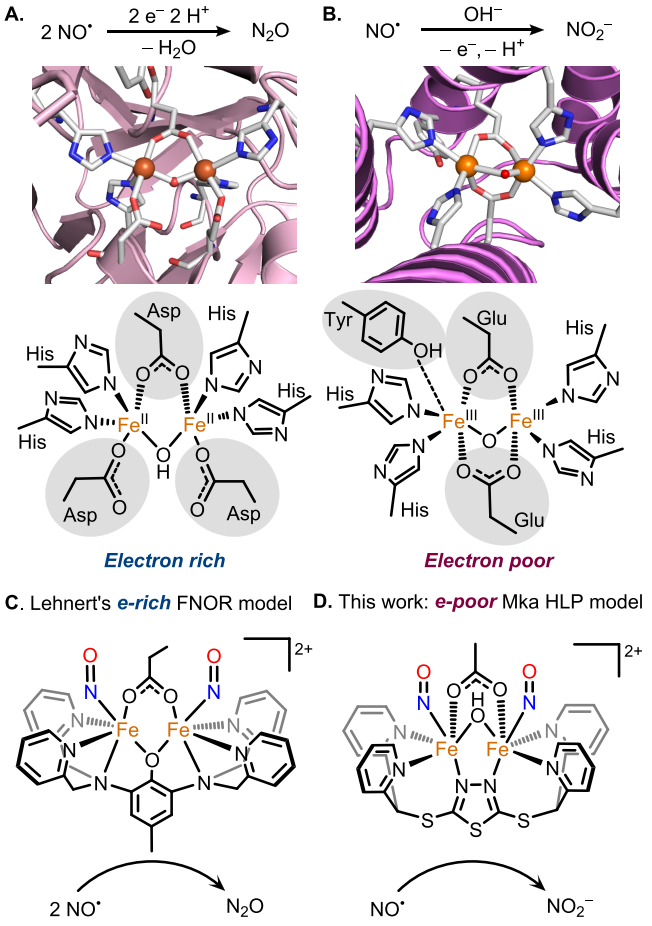

Figure 1. Diiron active site of (A) *T. maritima* FNOR enzyme (PDB: 1VME), and (B) *Mka*-HLP (PDB: 6Q09). (C) Previous example of a synthetic model of FNORs by Lehnert, and (D) the synthetic model of *Mka*-HLP in this work.

studies, nonheme diiron enzymes were not known to participate in the interconversion of NO• and nitrite.

Although the three diiron proteins perform distinct reactions, the diiron sites in FNORs, *Mka*-HLP, and YtfE all reside in histidine- and carboxylate-rich environments. The main difference between the FNOR and HLP diiron sites is that the HLPs possess a tyrosine ligand ca. 3.0 Å from the iron centers in place of a third carboxylate ligand (Figure 1A,B). Due to the long Tyr···Fe distance,[39] *Mka*-HLP and YtfE would be expected to be less electron-rich than the NO•-reducing FNOR site. Given that most small-molecule model systems have primarily focused on the synthesis of electron-rich diiron complexes to mimic the NO• reduction capabilities of the FNOR enzymes, we sought to develop an electron-deficient diiron model to mimic the coordination environment of the diiron sites in *Mka*-HLP and YtfE and study the mechanism of NO• oxidation at the diiron sites.

Herein, we report the synthesis and characterization of a new diiron complex that models the active sites of *Mka*-HLP and YtfE. The diferrous precursor ($\mathbf{Fe^{II}Fe^{II}}$) contains a single symmetric bridging acetate ligand and a bridging hydroxo moiety (Figure 1D). $\mathbf{Fe^{II}Fe^{II}}$ reacts with NO• to form a diiron dinitrosyl complex ($\{\mathbf{FeNO}\}^7_2$. In solution, $\{\mathbf{FeNO}\}^7_2$ releases NO• and converts to a rare mononitrosyl diiron complex $\mathbf{Fe^{II}\{FeNO\}^7}$. Furthermore, oxidation of $\{\mathbf{FeNO}\}^7_2$ leads to the formation of nitrite in 71% yield, while oxidation of the mononitrosyl complex $\mathbf{Fe^{II}\{FeNO\}^7}$ produces nitrite in only 9% yield. This work provides the first model study that reproduces the NO• oxidase reactivity by *Mka*-HLP and suggests the intermediacy of a $\{\mathbf{FeNO}\}^6/\{\mathbf{FeNO}\}^7$ species during the oxidation of NO• to nitrite.

RESULTS AND DISCUSSION

Synthesis and Characterization of the Diferrous Precursor $\mathbf{Fe^{II}Fe^{II}}$. In this study, we employ the previously reported Py_4DMcT ligand (**L**, Scheme 1)[41] to synthesize a diiron complex with a coordination environment similar to the diiron sites in *Mka*-HLP and YtfE, where each iron is coordinated to two histidines, bridged by two carboxylates, and a bridging O^{2-}/OH^- ligand. Treatment of Py_4DMcT with two equivalents of bis-acetonitrile iron(II) triflate ($Fe^{II}(OTf)_2MeCN_2$), one equivalent of TBAOAc, and one equivalent of TBAOH (TBA = tetrabutylammonium) in acetonitrile affords a red complex. Vapor diffusion of diethyl ether into the acetonitrile solution afforded red crystals in 60% yield (Scheme 1).

Single-crystal X-ray diffraction (XRD) reveals the diiron complex $[\mathbf{L}Fe^{II}_2(OH)(OAc)(MeCN)_2](OTf)_2$ ($\mathbf{Fe^{II}Fe^{II}}$) (see

Scheme 1. Synthesis of Diferrous Precursor

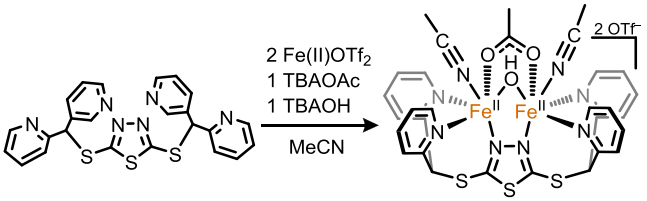

the Supporting Information, Figure S84). Both iron centers reside in octahedral coordination environments composed of three N donors, one μ-1,3 bridging acetate, and one μ-1,1 bridging hydroxo. Each Fe^{II} center contains an additional open coordination site occupied by acetonitrile solvent molecules (Scheme 1, Figure S84). Mössbauer spectroscopy reveals the presence of two equivalent high-spin Fe^{II} centers, with an isomer shift (δ) of 1.20 mm s^{-1} and a quadrupole splitting (ΔE_Q) of 2.49 mm s^{-1} (Figure S1). ^{1}H NMR spectrum of $\mathbf{Fe^{II}Fe^{II}}$ in MeCN-d_3 shows many broad resonances from 90 to −20 ppm (Figure S2).

Synthesis and Characterization of the Diiron Dinitrosyl Complex $\{\mathbf{FeNO}\}^7_2$. Following the successful isolation and characterization of $\mathbf{Fe^{II}Fe^{II}}$, we examined its reactivity toward NO•. The reaction between $\mathbf{Fe^{II}Fe^{II}}$ and NO• was monitored by using UV−vis spectroscopy at −40 °C in various solvents, including dichloromethane, MeCN, and acetone. Addition of excess NO• (14 equiv) to $\mathbf{Fe^{II}Fe^{II}}$ affords a dark brown species with UV−vis absorption bands at 455 nm (ε = 1690−1630 M^{-1} cm^{-1}) and 610 nm (ε = 530−490 M^{-1} cm^{-1}) (Figure 2A, Figures S17−S19).

X-ray quality single crystals of the dark brown product were grown from a dichloromethane/diethyl ether solution at −35 °C. X-ray diffraction (XRD) analysis reveals a diiron dinitrosyl species $[\mathbf{L}Fe^{II}(OAc)(OH)(NO)_2][OTf]_2$ species ($\{\mathbf{FeNO}\}^7_2$). The pseudooctahedral coordination environment around each Fe^{II} center in the starting material is retained, with nitrosyl ligands replacing the acetonitrile molecules (Figure 2B). Comparison of the structures of $\{\mathbf{FeNO}\}^7_2$ and $\mathbf{Fe^{II}Fe^{II}}$

https://doi.org/10.1021/jacs.3c05155
J. Am. Chem. Soc. 2023, 145, 22993−22999

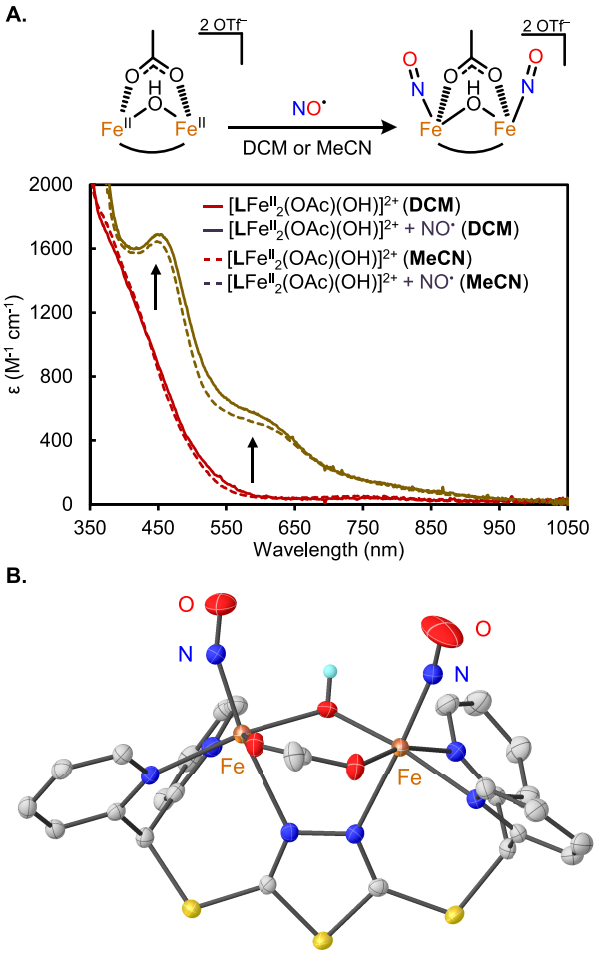

Figure 2. (A) In situ UV−vis spectra of the treatment of a 0.5 mM solution of $\mathbf{Fe^{II}Fe^{II}}$ with an excess (14 equiv) of NO• at −40 °C in dichloromethane (solid lines) or acetonitrile (dashed lines). (B) Solid-state structure of $\mathbf{\{FeNO\}^7_2}$. Thermal ellipsoids are shown at the 80% level of probability, and the outer sphere triflate counteranions and solvent molecules are omitted for clarity.

indicates that the Fe−Fe distance lengthens from 3.333 Å in $\mathbf{Fe^{II}Fe^{II}}$ to 3.455 Å in $\mathbf{\{FeNO\}^7_2}$. Additionally, $\mathbf{\{FeNO\}^7_2}$ displays Fe−NO bond lengths of 1.791(3) Å/1.781(3) Å and N−O bond distances of 1.133(4) Å/1.110(7) Å, typical for $\{FeNO\}^7$ species.[22−30,33]

Solid-state infrared (IR) spectroscopy of $\mathbf{\{FeNO\}^7_2}$ shows a broad N=O stretch at 1762 cm^{-1} that shifts to 1731 cm^{-1} upon ^{15}N-labeling (Figures S3 and S7). This value agrees with the N=O stretching frequencies reported for $\{FeNO\}^7$ complexes (∼1700−1800 cm^{-1}).[22−30,33] Mössbauer spectroscopy of $\mathbf{\{FeNO\}^7_2}$ exhibits an unsymmetric doublet commonly observed in $\{FeNO\}^7$ complexes,[42] with an isomer shift of δ = 0.72 mm/s and a quadrupole splitting value of ΔE_Q = 1.11 mm/s (Figure S6).

Synthesis and Characterization of the Diiron Mononitrosyl Complex $\mathbf{Fe^{II}\{FeNO\}^7}$. In contrast to the thermal stability typically displayed by $\{FeNO\}^7$ species, we found that $\mathbf{\{FeNO\}^7_2}$ spontaneously releases NO• in solution. In dichloromethane, the UV−vis features at 455 and 610 nm of $\mathbf{\{FeNO\}^7_2}$ decay as the temperature increases from −80 to 20 °C and then return to the same absorbance values as the temperature decreases back to −80 °C (Figure S20). Titration of NO• into a solution of $\mathbf{Fe^{II}Fe^{II}}$ indicates that full conversion of $\mathbf{Fe^{II}Fe^{II}}$ to $\mathbf{\{FeNO\}^7_2}$ requires more than two equivalents of NO• (Figures S22 and S23).

We turned to in situ infrared (IR) spectroscopy to further investigate the reversible binding of NO•. When $\mathbf{\{FeNO\}^7_2}$ was dissolved in dichloromethane at room temperature, a new ^{15}N-sensitive IR stretch at 1742(−30) cm^{-1} was observed (Figure 3A, blue trace). Upon the addition of an excess amount of NO•, the peak at 1742 cm^{-1} gradually decreased, and the NO• stretch at 1777 cm^{-1} associated with $\mathbf{\{FeNO\}^7_2}$ reappeared (Figure 3A, brown trace). Therefore, we tentatively assigned the peak at 1742 cm^{-1} to a mononitrosyl $\mathbf{Fe^{II}\{FeNO\}^7}$ species. Titration of NO• to a solution of $\mathbf{Fe^{II}\{FeNO\}^7}$ at −80 °C monitored by in situ IR spectroscopy allowed us to determine an equilibrium constant K_{eq} = 0.15 ± 0.02 M^{-1} for the mononitrosyl/dinitrosyl equilibrium (Scheme 2, see Supporting Information, Figures S26−S28).

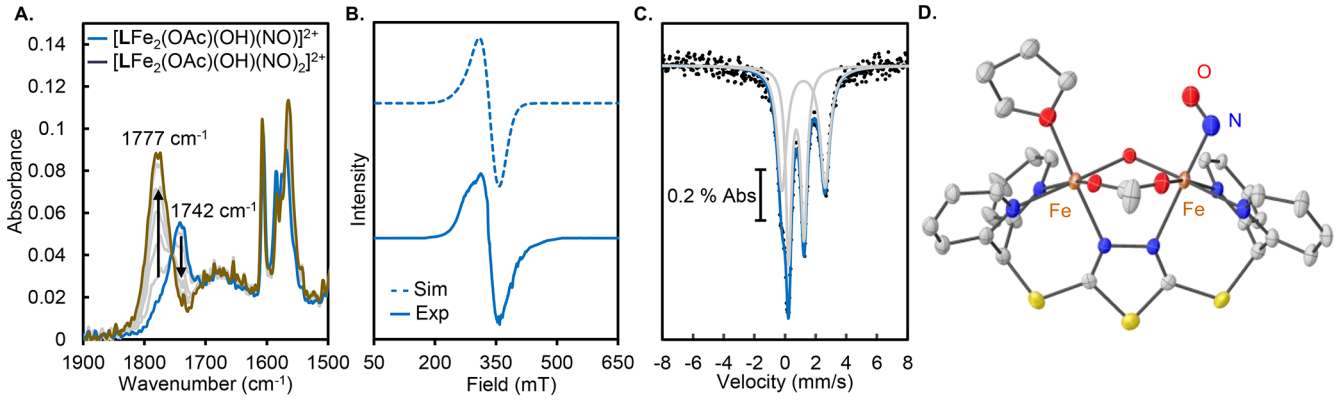

Figure 3. (A) In situ IR spectra of a titration of a 50 mM solution of $[\mathbf{LFe^{II}_2}(OAc)(OH)(NO)]^{2+}$ (blue trace) with 6 equiv NO• to form $[\mathbf{LFe^{II}_2}(OAc)(OH)(NO)_2]^{2+}$ (brown trace). Each trace after the initial blue trace is recorded after the addition of 1 eq. NO•. (B) X-band EPR spectrum of a 1 mM solution of $[\mathbf{LFe^{II}_2}(OAc)(OH)(NO)]^{2+}$ measured at 5 K in frozen CH_2Cl_2. Experimental parameters: frequency (ν) = 9.373 GHz; power = 2.000 mW; modulation amplitude = 5 G. Simulation parameters: $g_x = g_y = 1.977$, $g_z = 2.220$, line width half max 40 mT. (C) Solid-state Mössbauer spectrum of $[\mathbf{LFe^{II}_2}(OAc)(OH)(NO)]^{2+}$ (natural abundance) at 4 K and 0 T. (D) Single-crystal structure of $[\mathbf{LFe^{II}_2}(OAc)(OH)(NO)]^{2+}$, shown with 50% probability ellipsoids. Outer sphere triflate anions and solvent molecules are omitted for clarity. The bridging O ligand is hydroxy; however, the H atom is not shown.

https://doi.org/10.1021/jacs.3c05155
J. Am. Chem. Soc. 2023, 145, 22993−22999

Scheme 2. Equilibrium between Mononitrosyl and Dinitrosyl Diiron Species

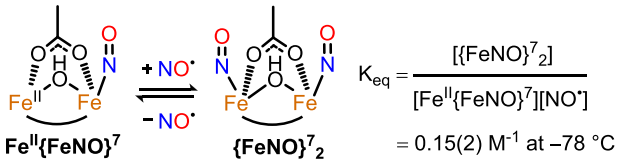

X-ray quality single crystals of the mononitrosyl complex were obtained by slow diffusion of THF into a dichloromethane solution of $\mathbf{Fe^{II}\{FeNO\}^7}$. The pure $\mathbf{Fe^{II}\{FeNO\}^7}$ sample can be prepared by the dissolution of $\mathbf{\{FeNO\}^7_2}$ at room temperature, followed by solvent removal *in vacuo* to remove the free NO•. Single crystal XRD analysis (Figure 3D) shows that one Fe^{II} center is coordinated by a THF solvent molecule, and the other is coordinated by NO•. The average Fe···Fe distance in $\mathbf{Fe^{II}\{FeNO\}^7}$ is 3.346 Å, falling in between that of $\mathbf{Fe^{II}Fe^{II}}$ (3.333 Å) and $\mathbf{\{FeNO\}^7_2}$ (3.455 Å). The Fe−NO bond length in $\mathbf{Fe^{II}\{FeNO\}^7}$ is 1.90(3) Å, significantly longer than those in $\mathbf{\{FeNO\}^7_2}$ (1.791(3) Å/1.781(3) Å), indicating a weaker interaction between Fe center and the nitrosyl ligand. The Fe−N−O unit in $\mathbf{Fe^{II}\{FeNO\}^7}$ is also more bent than those in $\mathbf{\{FeNO\}^7_2}$, displaying angles of 106.9 and 118.9° versus 153.5 and 156.4°, respectively. The highly bent Fe−N−O motif is unusual; it could be due to solid-state packing as no significant hydrogen bonding was observed.

An EPR spectrum of $\mathbf{Fe^{II}\{FeNO\}^7}$ in dichloromethane at 5 K in frozen CH_2Cl_2 displays a broad $S = 1/2$ signal at $g = 2.058$ (Figure 3B, Figure S41). This signal is similar to the EPR signal of $Fe^{II}\{FeNO\}^7$ species reported by Majumdar et al. with a g-value at 1.97.[26,27] Mössbauer spectroscopy of a crystalline sample of $\mathbf{Fe^{II}\{FeNO\}^7}$ reveals two iron centers in a 1:1 ratio (Figure 3C): one high-spin Fe^{II} with an isomer shift of $\delta = 1.20$ mm s^{-1} and quadrupole splitting $|\Delta E_Q| = 2.83$ mm s^{-1}, and one $\{FeNO\}^7$ moiety with an isomer shift $\delta = 0.74$ mms^{-1} and quadrupole splitting $|\Delta E_Q| = 1.01$ mm s^{-1}. These values are also comparable to the $\mathbf{Fe^{II}\{FeNO\}^7}$ complex reported by Majumdar et al.[26,27]

Diiron mononitrosyl complexes are rare in the literature due to the typically high affinity of ferrous centers toward NO•. $\mathbf{Fe^{II}\{FeNO\}^7}$ is the third example of a diiron mononitrosyl complex. The other two examples were reported by Majumdar and Lehnert via either selective delivery of a single equivalent of NO^+,[26] or blocking one NO• binding site using an unsymmetric ligand.[43] Our diiron complex prefers coordination of only one equivalent of NO•, despite the presence of open coordination sites on each Fe^{II} center. Notably, Majumdar et al. also structurally characterized both mononitrosyl and dinitrosyl diiron complexes. In their case, however, the Fe−NO distance, N=O distance, and Fe−N−O bond angles remain essentially the same in the mononitrosyl and the dinitrosyl structures.[26,27] The geometric differences of the Fe−NO moiety observed in $\mathbf{\{FeNO\}^7_2}$ and $\mathbf{Fe^{II}\{FeNO\}^7}$ suggest cooperativity in NO• binding. This may result from the electronic interactions between the two Fe centers due to the μ−OH and μ-OAc ligands, which are shared by the diiron sites in *Mka* HLP and YtfE.

Nitrite Formation from the Oxidation of $\mathbf{\{FeNO\}^7_2}$. With the fully characterized diiron mononitrosyl and dinitrosyl in hand, we sought to investigate their ability to reproduce the NO• detoxification reactivity of nonheme diiron proteins. Cyclic voltammetry (CV) studies of $\mathbf{\{FeNO\}^7_2}$ and $\mathbf{Fe^{II}\{FeNO\}^7}$ indicate that both complexes undergo an irreversible reduction at −1.3 and −1.05 V versus the Fc/Fc^+ couple, respectively (Figures S14−S16). Notably, in comparison to the redox couples of the previously reported N_2O-producing complexes by Lehnert et al. and Majumdar et al., the reduction of $\mathbf{\{FeNO\}^7_2}$ is shifted cathodically by ca. 200 mV.[22,27]

Gas chromatography (GC) analysis of a reaction between $\mathbf{\{FeNO\}^7_2}$ and cobaltocene showed no N_2O (g) formation. Analysis of the reaction mixture by EPR and IR did not show conclusive evidence for the formation of dinitrosyl iron complex (DNIC) or $Fe_2(NO)_2$ diamond core species (see Supporting Information).[44] It has been previously shown by Lehnert et al.[24,25,45] and Meyer et al.[33] that an electron-rich environment and a close N···N distance are crucial for efficient N_2O production. The electron-poor nature of the Py_4DMcT ligand as well as the long N···N distance in $\mathbf{\{FeNO\}^7_2}$ (4.750 Å versus 2.803 Å in the case of Lehnert et al.[24,25,45]), likely hinders the formation of the N−N bond necessary for N_2O production.

We next investigated the possibility of nitrite formation from the oxidation of $\mathbf{\{FeNO\}^7_2}$ and $\mathbf{Fe^{II}\{FeNO\}^7}$. In *Mka*-HLP, NO• oxidation to nitrite is thought to proceed through a radical attack at the μ-oxo bridge by NO• without formation of a $\{FeNO\}^6$ intermediate (Scheme 3A) or via a nucleophilic attack of a $\{FeNO\}^6$ intermediate by H_2O (Scheme 3B).[39,40] The reverse reaction−reduction of nitrite to NO• catalyzed by YtfE was proposed to go through a similar $\{FeNO\}^6$ intermediate but in the reverse direction (Scheme 3C).[35,36] In both cases, spectroscopic characterization of the $\{FeNO\}^6$ intermediate is limited or absent. As our diiron dinitrosyl complex shares a coordination environment similar to those of *Mka*-HLP and YtfE, we believed our diiron nitrosyl model complexes could generate nitrite upon oxidation. Cyclic

Scheme 3. (A) In situ IR spectra of the treatment of a 50.0 mM solution of $\mathbf{\{FeNO\}^7_2}$ (brown trace) with one equivalent of $[NAr_3][PF_6]$ at −78 °C in dichloromethane to form a putative $\mathbf{\{FeNO\}^6\{FeNO\}^7}$ species (red trace). The reaction was monitored by recording a spectrum every minute for 120 min

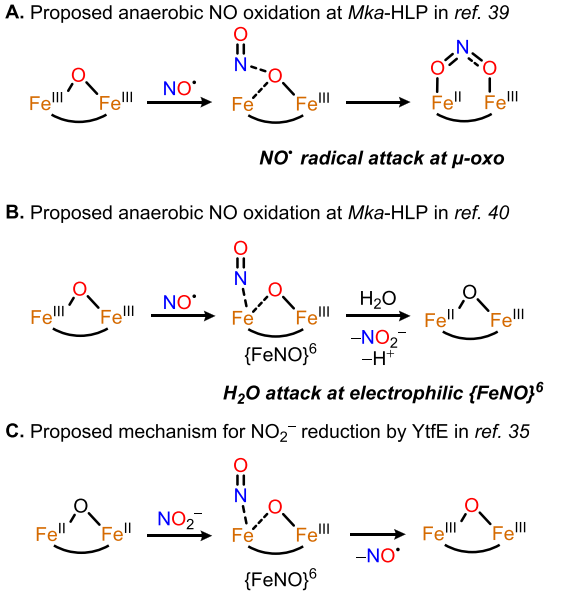

https://doi.org/10.1021/jacs.3c05155
J. Am. Chem. Soc. 2023, 145, 22993−22999

voltammetry studies indicate that both $\{\mathbf{FeNO}\}^7_2$ and $\mathbf{Fe^{II}}\{\mathbf{FeNO}\}7$ exhibit two irreversible oxidation events: 0.1 V, 0.3 V vs Fc/Fc^+ for $\{\mathbf{FeNO}\}^7_2$ and 0.4 V, 0.6 V for $\mathbf{Fe^{II}}\{\mathbf{FeNO}\}^7$ (SI, Figures S14−S16). Therefore, we selected tris(4-bromophenyl)-aminium hexafluorophosphate ($[NAr_3][PF_6]$, Magic Blue) with an $E_{1/2}$ = 0.66 V (vs $Ag/AgNO_3$) as the oxidant. Reaction of $\{\mathbf{FeNO}\}^7_2$ with one equivalent of $[NAr_3][PF_6]$ at −80 °C leads to the formation of a new species with a major absorbance at 420 nm (ε = 3400 M^{-1} cm^{-1}) and a weak transition at 1000 nm (ε = 270 M^{-1} cm^{-1}, Figure S24). Treatment of $\mathbf{Fe^{II}}\{\mathbf{FeNO}\}^7$ with $[NAr_3][PF_6]$ afforded a distinctly different spectrum that lacked the low-energy charge transfer band at 1000 nm (Figure S25). The products of both oxidation reactions are unstable above −80 °C, preventing isolation and full characterization.

With the promising initial results from the oxidation of $\{\mathbf{FeNO}\}^7_2$ and $\mathbf{Fe^{II}}\{\mathbf{FeNO}\}^7$, we turned to ion chromatography to quantify the nitrite production. A high yield of nitrite formation in 71% was observed from the oxidation of $\{\mathbf{FeNO}\}^7_2$ at −40 °C with an excess of NO• (Tables S1−S3 in the Supporting Information). Other conditions that favor the dissociation of NO• from $\{\mathbf{FeNO}\}^7_2$, such as higher temperature or low NO• concentrations, generally afford lower nitrite yields in the 30−51% range. The oxidation of the $\mathbf{Fe^{II}}\{\mathbf{FeNO}\}^7$ at −40 °C only produced nitrite in 9% yield. These studies suggest that $\{\mathbf{FeNO}\}^7_2$ is likely the active species for nitrite production. Importantly, control experiments without iron complexes show no nitrite production. Interestingly, $\{\mathbf{FeNO}\}^7_2$ without oxidant also produces nitrite in appreciable yield (24%). We speculate that this reactivity is perhaps associated with the disproportionation of $\{\mathbf{FeNO}\}^7_2$ to an Fe^{III} center and DNIC.[25] Indeed, nitrite production from $\mathbf{Fe^{II}Fe^{II}}$ was observed only in polar solvents, e.g., MeCN, which promotes disproportionation.

The formation of nitrite is also confirmed with ^{15}N NMR spectroscopy. Both $\{\mathbf{FeNO}\}^7_2$ and $\mathbf{Fe^{II}}\{\mathbf{FeNO}\}^7$ are ^{15}N NMR silent due to the proximity of the ^{15}N to the paramagnetic Fe centers. Oxidation of $\{\mathbf{Fe^{15}NO}\}^7_2$ with one equivalent of $[NAr_3]PF_6$ followed by warming up to room temperature resulted in an ^{15}N NMR spectrum with one peak at 242 ppm (see SI, Figure S80), which matches well with the ^{15}N signal of tetrabutylammonium nitrite-^{15}N at 244 ppm (Figure S79). Self-decomposition of $\{\mathbf{FeNO}\}^7_2$-^{15}N in MeCN-d_3 at room temperature also produced a nitrite signal at 248 ppm (Figures S81−S83).

Finally, to gain insight into the intermediate that produces nitrite, we monitored the oxidation of $\{\mathbf{FeNO}\}^7_2$ with in situ solution IR spectroscopy. Oxidation of $\{\mathbf{FeNO}\}^7_2$ with $[NAr_3]PF_6$ at −80 °C in CH_2Cl_2 led to two ^{15}N-sensitive peaks at 1777 (−34) cm^{-1} and 1816 (−34) cm^{-1}, suggesting the possible formation of an $\{\mathbf{FeNO}\}^6/\{\mathbf{FeNO}\}^7$ species (Figure 4, see SI, Figures S33 and S34). The only isolated high spin $\{FeNO\}^6$ complex in the literature was reported by the Lehnert group.[46,47] It exhibits an N=O stretch at 1879 cm^{-1}, which is significantly higher than its $\{FeNO\}^7$ analog at 1750 cm^{-1}. Although an $\{FeNO\}^6$ species was not observed in *Mka*-HLP and YtfE, our observation of $\{FeNO\}^6$ species and the resultant ON−O bond formation suggests the proposed involvement of an $\{FeNO\}^6$ species in the interconversion of nitrite and NO• is reasonable (Scheme 4).[35,36,39,40]

The EPR analysis of $\{\mathbf{FeNO}\}^6/\{\mathbf{FeNO}\}^7$ generated from in situ reaction of $\{\mathbf{FeNO}\}^7$ and Magic Blue shows an EPR signal around g = 4 (Figure S46), which was assigned as a high-spin

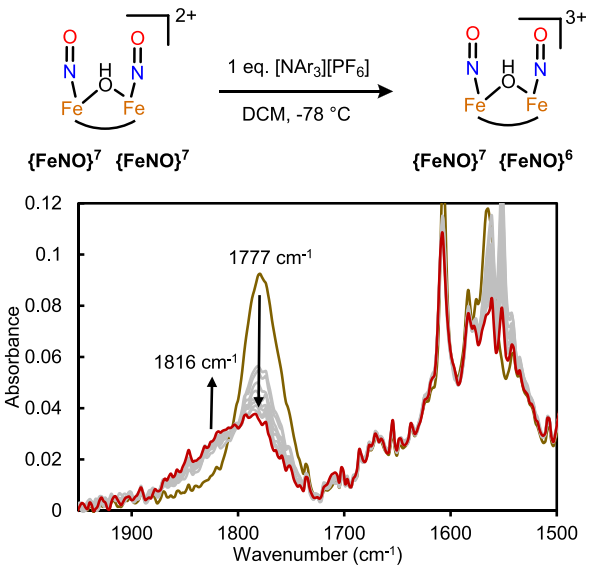

Figure 4. Proposed mechanism for NO•/nitrite interconversion at diiron cofactors.

Scheme 4. Proposed Mechanism for Anaerobic NO• Oxidation at $\{\mathbf{FeNO}\}^7_2$

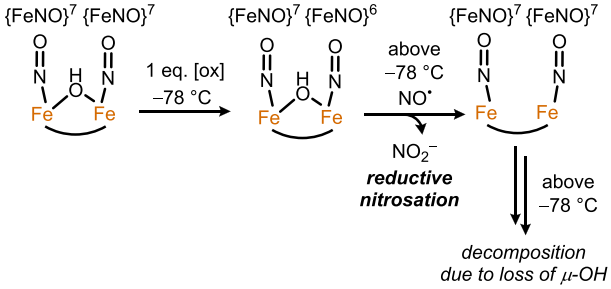

$\{FeNO\}^7$ species motif. At this point, we are unsure if the EPR signal is from $\{\mathbf{FeNO}\}^6/\{\mathbf{FeNO}\}^7$ or the diiron product after nitrite formation, since both species contain a $\{FeNO\}^7$ motif. Further warming the reaction mixture to room temperature resulted in an intractable mixture (Scheme 4). Unfortunately, we could not structurally characterize the high-spin $\{FeNO\}^7$ product after nitrite formation. We believe that the loss of the μ−OH ligand leads to an unstable diiron construct that causes ligand decomposition.

CONCLUSIONS

In summary, we have developed a new diiron model system that can support the reversible binding of NO• between diiron dinitrosyl species $\{\mathbf{FeNO}\}^7_2$ and diiron mononitrosyl species $\mathbf{Fe^{II}}\{\mathbf{FeNO}\}^7$. Both $\{\mathbf{FeNO}\}^7_2$ and $\mathbf{Fe^{II}}\{\mathbf{FeNO}\}^7$ have been fully characterized by XRD, EPR, IR, and Mössbauer spectroscopy. Only two other diiron mononitrosyl species have been reported. The preferential coordination of one equivalent of NO• to the diiron complex to form the mononitrosyl species when each Fe^{II} center possesses an open coordination site is unprecedented. Inspired by the recent discovery of the electron-poor diiron site in *Mka*-HLP that mediates the oxidation of NO• to nitrite, we found that our $\{\mathbf{FeNO}\}^7_2$ complex can also generate nitrite in 71% yield upon one-electron oxidation. Oxidation of the corresponding mononitrosyl $\mathbf{Fe^{II}}\{\mathbf{FeNO}\}^7$ species shows the formation of nitrite; however, the yield is greatly diminished, suggesting that

https://doi.org/10.1021/jacs.3c05155
J. Am. Chem. Soc. 2023, 145, 22993−22999

the dinitrosyl complex is the more likely intermediate for nitrite formation. Investigation of this $NO^{\bullet}$ oxidation reaction with in situ solution IR spectroscopy suggests the intermediacy of an $\{FeNO\}^6/\{FeNO\}^7$ species.

■ ASSOCIATED CONTENT

Supporting Information

The Supporting Information is available free of charge at https://pubs.acs.org/doi/10.1021/jacs.3c05155.

Materials, details of synthesis and characterization, spectroscopic studies, and crystallographic data for $Fe^{II}Fe^{II}$ (2263715), $\{FeNO\}_2^7$(2263716), and $Fe^{II}\{FeNO\}^7$ (2263715) (PDF)

Accession Codes

CCDC 2263715−2263717 contain the supplementary crystallographic data for this paper. These data can be obtained free of charge via www.ccdc.cam.ac.uk/data_request/cif, or by emailing data_request@ccdc.cam.ac.uk, or by contacting The Cambridge Crystallographic Data Centre, 12 Union Road, Cambridge CB2 1EZ, UK; fax: +44 1223 336033.

■ AUTHOR INFORMATION

Corresponding Author

Shiyu Zhang − *Department of Chemistry & Biochemistry, The Ohio State University, Columbus, Ohio 43210, United States;* orcid.org/0000-0002-2536-4324; Email: zhang.8941@osu.edu

Authors

Anna L. Poptic − *Department of Chemistry & Biochemistry, The Ohio State University, Columbus, Ohio 43210, United States*

Jeffrey K. Klinger − *Department of Chemistry & Biochemistry, The Ohio State University, Columbus, Ohio 43210, United States*

Samantha L. Carter − *Department of Chemistry & Biochemistry, The Ohio State University, Columbus, Ohio 43210, United States*

Curtis E. Moore − *Department of Chemistry & Biochemistry, The Ohio State University, Columbus, Ohio 43210, United States*

Complete contact information is available at: https://pubs.acs.org/10.1021/jacs.3c05155

Notes

The authors declare no competing financial interest.

■ ACKNOWLEDGMENTS

This publication is based on work funded by the National Science Foundation under award no. CHE-2246440 and by a Pelotonia Graduate Fellowship awarded to A.L.P. The authors acknowledge The Ohio State University Department of Chemistry and Biochemistry for additional financial support and resources.

■ REFERENCES

(1) Ignarro, L. J. *Nitric Oxide: Biology and Pathobiology*; Elsevier: Amsterdam, 2009.

(2) Toledo, J. C.; Augusto, O. Connecting the Chemical and Biological Properties of Nitric Oxide. *Chem. Res. Toxicol.* **2012**, *25*, 975−989.

(3) Bogdan, C. Nitric Oxide and the Immune Response - Nature Immunology. *Nat. Immunol.* **2001**, *2*, 907−916.

(4) Missall, T. A.; Lodge, J. K.; McEwen, J. E. Mechanisms of Resistance to Oxidative and Nitrosative Stress: Implications for Fungal Survival in Mammalian Hosts. *Eukaryot. Cell* **2004**, *3*, 835−846.

(5) Justino, M. C.; Almeida, C. C.; Gonçalves, V. L.; Teixeira, M.; Saraiva, L. M. Escherichia Coli YtfE Is a Di-Iron Protein with an Important Function in Assembly of Iron−Sulphur Clusters. *FEMS Microbiol. Lett.* **2006**, *257*, 278−284.

(6) Justino, M. C.; Almeida, C. C.; Teixeira, M.; Saraiva, L. M. Escherichia Coli Di-Iron YtfE Protein Is Necessary for the Repair of Stress-Damaged Iron-Sulfur Clusters. *J. Biol. Chem.* **2007**, *282*, 10352−10359.

(7) Mills, P. C.; Rowley, G.; Spiro, S.; Hinton, J. C.; Richardson, D. J. A Combination of Cytochrome c Nitrite Reductase (NrfA) and Flavorubredoxin (NorV) Protects Salmonella Enterica Serovar Typhimurium against Killing by NO in Anoxic Environments. *Microbiology* **2008**, *154*, 1218−1228.

(8) Rohde, K. H.; Abramovitch, R. B.; Russell, D. G. Mycobacterium Tuberculosis Invasion of Macrophages: Linking Bacterial Gene Expression to Environmental Cues. *Cell Host Microbe* **2007**, *2*, 352−364.

(9) Flint, A.; Stintzi, A.; Saraiva, L. M. Oxidative and Nitrosative Stress Defences of Helicobacter and Campylobacter Species That Counteract Mammalian Immunity. *FEMS Microbiol. Rev.* **2016**, *40*, 938−960.

(10) Frederick, R. E.; Caranto, J. D.; Masitas, C. A.; Gebhardt, L. L.; MacGowan, C. E.; Limberger, R. J.; Kurtz, D. M. Dioxygen and Nitric Oxide Scavenging by Treponema Denticola Flavodiiron Protein: A Mechanistic Paradigm for Catalysis. *J. Biol. Inorg. Chem.* **2015**, *20*, 603−613.

(11) Eriksson, S.; Lucchini, S.; Thompson, A.; Rhen, M.; Hinton, J. C. D. Unravelling the Biology of Macrophage Infection by Gene Expression Profiling of Intracellular Salmonella Enterica. *Mol. Microbiol.* **2003**, *47*, 103−118.

(12) Rodrigues, R.; Vicente, J. B.; Félix, R.; Oliveira, S.; Teixeira, M.; Rodrigues-Pousada, C. Desulfovibrio Gigas Flavodiiron Protein Affords Protection against Nitrosative Stress in Vivo. *J. Bacteriol.* **2006**, *188*, 2745−2751.

(13) Stevanin, T. M.; Moir, J. W. B.; Read, R. C. Nitric Oxide Detoxification Systems Enhance Survival of Neisseria Meningitidis in Human Macrophages and in Nasopharyngeal Mucosa. *Infect. Immun.* **2005**, *73*, 3322−3329.

(14) Khatua, S.; Majumdar, A. Flavodiiron Nitric Oxide Reductases: Recent Developments in the Mechanistic Study and Model Chemistry for the Catalytic Reduction of NO. *J. Inorg. Biochem.* **2015**, *142*, 145−153.

(15) Martins, M. C.; Romão, C. V.; Folgosa, F.; Borges, P. T.; Frazão, C.; Teixeira, M. How Superoxide Reductases and Flavodiiron Proteins Combat Oxidative Stress in Anaerobes. *Free Radic. Biol. Med.* **2019**, *140*, 36−60.

(16) Kurtz, D. M. Flavo-Diiron Enzymes: Nitric Oxide or Dioxygen Reductases? *Dalt. Trans.* **2007**, *37*, 4115−4121.

(17) Hayashi, T.; Caranto, J. D.; Matsumura, H.; Kurtz, D. M.; Moënne-Loccoz, P. Vibrational Analysis of Mononitrosyl Complexes in Hemerythrin and Flavodiiron Proteins: Relevance to Detoxifying No Reductase. *J. Am. Chem. Soc.* **2012**, *134*, 6878−6884.

(18) Caranto, J. D.; Weitz, A.; Hendrich, M. P.; Kurtz, D. M. The Nitric Oxide Reductase Mechanism of a Flavo-Diiron Protein: Identification of Active-Site Intermediates and Products. *J. Am. Chem. Soc.* **2014**, *136*, 7981−7992.

(19) Hayashi, T.; Caranto, J. D.; Wampler, D. A.; Kurtz, D. M.; Moënne-Loccoz, P. Insights into the Nitric Oxide Reductase Mechanism of Flavodiiron Proteins from a Flavin-Free Enzyme. *Biochemistry* **2010**, *49*, 7040−7049.

(20) Lehnert, N.; Kim, E.; Dong, H. T.; Harland, J. B.; Hunt, A. P.; Manickas, E. C.; Oakley, K. M.; Pham, J.; Reed, G. C.; Alfaro, V. S. The Biologically Relevant Coordination Chemistry of Iron and Nitric

Oxide: Electronic Structure and Reactivity. *Chem. Rev.* **2021**, *121*, 14682−14905.
(21) Pal, N.; Jana, M.; Majumdar, A. Reduction of NO by Diiron Complexes in Relation to Flavodiiron Nitric Oxide Reductases. *Chem. Commun.* **2021**, *57*, 8682−8698.
(22) Zheng, S.; Berto, T. C.; Dahl, E. W.; Hoffman, M. B.; Speelman, A. L.; Lehnert, N. The Functional Model Complex $[Fe_2(BPMP)(OPr)(NO)_2](BPh_4)_2$ Provides Insight into the Mechanism of Flavodiiron NO Reductases. *J. Am. Chem. Soc.* **2013**, *135*, 4902−4905.
(23) White, C. J.; Speelman, A. L.; Kupper, C.; Demeshko, S.; Meyer, F.; Shanahan, J. P.; Alp, E. E.; Hu, M.; Zhao, J.; Lehnert, N. The Semireduced Mechanism for Nitric Oxide Reduction by Non-Heme Diiron Complexes: Modeling Flavodiiron Nitric Oxide Reductases. *J. Am. Chem. Soc.* **2018**, *140*, 2562−2574.
(24) Dong, H. T.; White, C. J.; Zhang, B.; Krebs, C.; Lehnert, N. Non-Heme Diiron Model Complexes Can Mediate Direct NO Reduction: Mechanistic Insight into Flavodiiron NO Reductases. *J. Am. Chem. Soc.* **2018**, *140*, 13429−13440.
(25) White, C. J.; Lengel, M. O.; Bracken, A. J.; Kampf, J. W.; Speelman, A. L.; Alp, E. E.; Hu, M. Y.; Zhao, J.; Lehnert, N. Distortion of the [FeNO]2 Core in Flavodiiron Nitric Oxide Reductase Models Inhibits N-N Bond Formation and Promotes Formation of Unusual Dinitrosyl Iron Complexes: Implications for Catalysis and Reactivity. *J. Am. Chem. Soc.* **2022**, *144*, 3804−3820.
(26) Jana, M.; Pal, N.; White, C. J.; Kupper, C.; Meyer, F.; Lehnert, N.; Majumdar, A. Functional Mononitrosyl Diiron(II) Complex Mediates the Reduction of NO to N_2O with Relevance for Flavodiiron NO Reductases. *J. Am. Chem. Soc.* **2017**, *139*, 14380−14383.
(27) Jana, M.; White, C. J.; Pal, N.; Demeshko, S.; Cordes, C.; Meyer, F.; Lehnert, N.; Majumdar, A. Functional Models for the Mono- And Dinitrosyl Intermediates of FNORs: Semireduction versus Superreduction of NO. *J. Am. Chem. Soc.* **2020**, *142*, 6600−6616.
(28) Pal, N.; White, C. J.; Demeshko, S.; Meyer, F.; Lehnert, N.; Majumdar, A. A Monohydrosulfidodinitrosyldiiron Complex That Generates N_2O as a Model for Flavodiiron Nitric Oxide Reductases: Reaction Mechanism and Electronic Structure. *Inorg. Chem.* **2021**, *60*, 15890−15900.
(29) Feig, A. L.; Bautista, M. T.; Lippard, S. J. A Carboxylate-Bridged Non-Heme Diiron Dinitrosyl Complex. *Inorg. Chem.* **1996**, *35*, 6892−6898.
(30) Majumdar, A.; Lippard, S. J. Non-Heme Mononitrosyldiiron Complexes: Importance of Iron Oxidation State in Controlling the Nature of the Nitrosylated Products. *Inorg. Chem.* **2013**, *52*, 13292−13294.
(31) Wu, W.-Y.; Tsai, M.-L.; Lai, Y.-A.; Hsieh, C.-H.; Liaw, W.-F. NO Reduction to N_2O Triggered by a Dinuclear Dinitrosyl Iron Complex via the Associated Pathways of Hyponitrite Formation and NO Disproportionation. *Inorg. Chem.* **2021**, *60*, 15874−15889.
(32) Wu, W.-Y.; Hsu, C.-N.; Hsieh, C.-H.; Chiou, T.-W.; Tsai, M.-L.; Chiang, M.-H.; Liaw, W.-F. NO to $[N_2O_2]^{2-}$ to N_2O Conversion Triggered by $\{Fe(NO)_2\}^{10}$-$\{Fe(NO)_2\}^9$ Dinuclear Dinitrosyl Iron Complex. *Inorg. Chem.* **2019**, *58*, 9586−9591.
(33) Kindermann, N.; Schober, A.; Demeshko, S.; Lehnert, N.; Meyer, F. Reductive Transformations of a Pyrazolate-Based Bioinspired Diiron-Dinitrosyl Complex. *Inorg. Chem.* **2016**, *55*, 11538−11550.
(34) Alvarez-Carreño, C.; Alva, V.; Becerra, A.; Lazcano, A. Structure, Function and Evolution of the Hemerythrin-like Domain Superfamily. *Protein Sci.* **2018**, *27*, 848−860.
(35) Crack, J. C.; Balasiny, B. K.; Bennett, S. P.; Rolfe, M. D.; Froes, A.; Macmillan, F.; Green, J.; Cole, J. A.; Le Brun, N. E. The Di-Iron Protein YtfE Is a Nitric Oxide-Generating Nitrite Reductase Involved in the Management of Nitrosative Stress. *J. Am. Chem. Soc.* **2022**, *144*, 7129−7145.
(36) Wang, J.; Vine, C. E.; Balasiny, B. K.; Rizk, J.; Bradley, C. L.; Tinajero-Trejo, M.; Poole, R. K.; Bergaust, L. L.; Bakken, L. R.; Cole, J. A. The Roles of the Hybrid Cluster Protein, Hcp and Its Reductase, Hcr, in High Affinity Nitric Oxide Reduction That Protects Anaerobic Cultures of Escherichia Coli against Nitrosative Stress. *Mol. Microbiol.* **2016**, *100*, 877−892.
(37) Ma, Z.; Strickland, K. T.; Cherne, M. D.; Sehanobish, E.; Rohde, K. H.; Self, W. T.; Davidson, V. L. The Rv2633c Protein of Mycobacterium Tuberculosis Is a Non-Heme Di-Iron Catalase with a Possible Role in Defenses against Oxidative Stress. *J. Biol. Chem.* **2018**, *293*, 1590−1595.
(38) Ma, Z.; Abendroth, J.; Buchko, G. W.; Rohde, K. H.; Davidson, V. L. Crystal Structure of a Hemerythrin-like Protein from Mycobacterium Kansasii and Homology Model of the Orthologous Rv2633c Protein of M. *Tuberculosis. Biochem. J.* **2020**, *477*, 567−581.
(39) Albert, T.; Moënne-Loccoz, P. Spectroscopic Characterization of a Diferric Mycobacterial Hemerythrin-Like Protein with Unprecedented Reactivity toward Nitric Oxide. *J. Am. Chem. Soc.* **2022**, *144*, 17611−17621.
(40) Ma, Z.; Holland, A. A.; Szlamkowicz, I.; Anagnostopoulos, V.; Nogueira, M. L. C.; Caranto, J. D.; Davidson, V. L. The Hemerythrin-like Diiron Protein from Mycobacterium Kansasii Is a Nitric Oxide Peroxidase. *J. Biol. Chem.* **2022**, *298*, No. 101696.
(41) Poptic, A. L.; Chen, Y. P.; Chang, T.; Chen, Y. S.; Moore, C. E.; Zhang, S. Site-Differentiated $Mn^{II}Fe^{II}$Complex Reproducing the Selective Assembly of Biological Heterobimetallic Mn/Fe Cofactors. *J. Am. Chem. Soc.* **2023**, *145*, 9.
(42) Gütlich, P.; Bill, E.; Trautwein, A. X. *Mössbauer Spectroscopy and Transition Metal Chemistry: Fundamentals and Applications*; Springer: Berlin Heidelberg, 2011.
(43) Dong, H. T.; Zong, Y.; Bracken, A. J.; Lengel, M. O.; Kampf, J. W.; Sil, D.; Krebs, C.; Lehnert, N. Synthesis and Characterization of a Model Complex for Flavodiiron NO Reductases That Stabilizes a Diiron Mononitrosyl Complex. *J. Inorg. Biochem.* **2022**, *229*, No. 111723.
(44) Dong, H. T.; Speelman, A. L.; Kozemchak, C. E.; Sil, D.; Krebs, C.; Lehnert, N. The Fe2(NO)2 Diamond Core: A Unique Structural Motif In Non-Heme Iron−NO Chemistry. *Angew. Chem., Int. Ed.* **2019**, *58*, 17695−17699.
(45) Dong, H. T.; Camarena, S.; Sil, D.; Lengel, M. O.; Zhao, J.; Hu, M. Y.; Alp, E. E.; Krebs, C.; Lehnert, N. What Is the Right Level of Activation of a High-Spin $\{FeNO\}^7$ Complex to Enable Direct N-N Coupling? Mechanistic Insight into Flavodiiron NO Reductases. *J. Am. Chem. Soc.* **2022**, *144*, 16395−16409.
(46) Speelman, A. L.; Zhang, B.; Krebs, C.; Lehnert, N. Structural and Spectroscopic Characterization of a High-Spin $\{FeNO\}^6$ Complex with an Iron(IV)-NO- Electronic Structure. *Angew. Chem., Int. Ed.* **2016**, *55*, 6685−6688.
(47) Speelman, A. L.; White, C. J.; Zhang, B.; Alp, E. E.; Zhao, J.; Hu, M.; Krebs, C.; Penner-Hahn, J.; Lehnert, N. Non-Heme High-Spin $\{FeNO\}^{6-8}$ Complexes: One Ligand Platform Can Do It All. *J. Am. Chem. Soc.* **2018**, *140*, 11341−11359.

https://doi.org/10.1021/jacs.3c05155
J. Am. Chem. Soc. 2023, 145, 22993−22999